



**HAL**  
open science

# Redesigning methionyl-tRNA synthetase for $\beta$ -methionine activity with adaptive landscape flattening and experiments

Vaitea Opuu, Giuliano Nigro, Christine Lazennec-Schurdevin, Yves Mechulam, Emmanuelle Schmitt, Thomas Simonson

## ► To cite this version:

Vaitea Opuu, Giuliano Nigro, Christine Lazennec-Schurdevin, Yves Mechulam, Emmanuelle Schmitt, et al.. Redesigning methionyl-tRNA synthetase for  $\beta$ -methionine activity with adaptive landscape flattening and experiments. *Protein Science*, 2023, 32 (9), 10.1002/pro.4738 . hal-04285116

**HAL Id: hal-04285116**


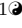
**<https://polytechnique.hal.science/hal-04285116>**

Submitted on 17 Nov 2023

**HAL** is a multi-disciplinary open access archive for the deposit and dissemination of scientific research documents, whether they are published or not. The documents may come from teaching and research institutions in France or abroad, or from public or private research centers.

L'archive ouverte pluridisciplinaire **HAL**, est destinée au dépôt et à la diffusion de documents scientifiques de niveau recherche, publiés ou non, émanant des établissements d'enseignement et de recherche français ou étrangers, des laboratoires publics ou privés.

# Redesigning methionyl-tRNA synthetase for $\beta$ -methionine activity with adaptive landscape flattening and experiments

Vaitea Opuu<sup>1</sup>, Giuliano Nigro<sup>1</sup>, Christine Lazennec-Schurdevin<sup>1</sup>, Yves Mechulam<sup>1\*</sup>, Emmanuelle Schmitt<sup>1\*</sup>, Thomas Simonson<sup>1\*</sup>

<sup>1</sup> Laboratoire de Biologie Structurale de la Cellule (CNRS UMR7654), Ecole Polytechnique, Institut Polytechnique de Paris, Palaiseau, France

 These authors contributed equally. \*Corresponding authors:

yves.mechulam@polytechnique.edu, emmanuelle.schmitt@polytechnique.edu,

thomas.simonson@polytechnique.edu

## Abstract

Amino acids (AAs) with a noncanonical backbone would be a valuable tool for protein engineering, enabling new structural motifs and building blocks. To incorporate them into an expanded genetic code, the first, key step is to obtain an appropriate aminoacyl-tRNA synthetase (aaRS). Currently, directed evolution is not available to optimize such AAs, since an appropriate selective pressure is not available.

Computational protein design (CPD) is an alternative. We used a new CPD method to redesign MetRS and increase its activity towards  $\beta$ -Met, which has an extra backbone methylene. The new method considered a few active site positions for design and used a Monte Carlo exploration of the corresponding sequence space. During the exploration, a bias energy was adaptively learned, such that the free energy landscape of the apo enzyme was flattened. Enzyme variants could then be sampled, in the presence of the ligand and the bias energy, according to their  $\beta$ -Met binding affinities. Eleven predicted variants were chosen for experimental testing; all exhibited detectable activity for  $\beta$ -Met adenylation. Top predicted hits were characterized experimentally in detail.

Dissociation constants, catalytic rates, and Michaelis constants for both  $\alpha$ -Met and

$\beta$ -Met were measured. The best mutant retained a preference for  $\alpha$ -Met over  $\beta$ -Met; however, the preference was reduced, compared to the wildtype, by a factor of 29. For this mutant, high resolution crystal structures were obtained in complex with both  $\alpha$ -Met and  $\beta$ -Met, indicating that the predicted, active conformation of  $\beta$ -Met in the active site was retained.

## Author summary

Amino acids (AAs) with a noncanonical backbone would be valuable for protein engineering, enabling new structural motifs. To incorporate them into an expanded genetic code, the key step is to obtain an appropriate aminoacyl-tRNA synthetase (aaRS). Currently, directed evolution is not available to optimize such AAs. Computational protein design is an alternative. We used a new method to redesign MetRS and increase its activity towards  $\beta$ -Met, which has an extra backbone methylene. The method considered a few active site positions for design and used a Monte Carlo exploration of sequence space, during which a bias energy was adaptively learned, such that the free energy landscape of the apo enzyme was flattened. Enzyme variants could then be sampled, in the presence of the ligand and the bias energy, according to their  $\beta$ -Met binding affinities. Eleven predicted variants were chosen for experimental testing; all exhibited detectable  $\beta$ -Met adenylation activity. Top hits were characterized experimentally in detail. The best mutant had its preference for  $\alpha$ -Met over  $\beta$ -Met reduced by a factor of 29. Crystal structures indicated that the predicted, active conformation of  $\beta$ -Met in the active site was retained.

## Introduction

Each aminoacyl-tRNA synthetase (aaRS) attaches a specific amino acid to a tRNA that carries the corresponding anticodon, establishing the genetic code [1]. The attachment involves two steps: the amino acid (AA) reacts first with ATP to form aminoacyl adenylate. Next, the adenylate reacts with tRNA. Several aaRSs have been engineered experimentally to accept noncanonical amino acids (ncAAs) as preferred substrates [2–6]. This is the key step to make the ncAA part of an expanded

1  
2  
3  
4  
5  
6  
7

code [3, 6, 7]. The ncAA can then be genetically encoded and incorporated into proteins by the cellular machinery. Thus, TyrRS was redesigned to be specific for several ncAAs [3, 6] and MetRS was redesigned to prefer azidonorleucine [8]. Several hundred ncAAs have been introduced into expanded codes, mostly using directed evolution to obtain the appropriate aaRSs. However, all these ncAAs had standard backbones.

In contrast, ncAAs with non standard backbones, such as D-AAAs or  $\beta$ -AAAs, would be of great interest in protein engineering, opening the possibility of new structural motifs and building blocks. For example,  $\beta$ -AAAs have an extra backbone methylene that increases backbone flexibility, alters helical propensities [9, 10], increases the distance between  $\alpha$  carbons, provides resistance to proteases, and can lead to modified side chain orientations in loop or sheet regions. To incorporate such ncAAs into an expanded code, the first step is to obtain an appropriate aaRS. However, directed evolution of aaRSs is still a major difficulty. The diversity one can explore and the selective pressure one can apply are limited, so the enzymes evolved so far have been weakly-active [11, 12]. In many situations, directed evolution is impossible, as no appropriate selective pressure can be applied. Thus, some archaeal tRNAs are not orthogonal to *E. coli*, precluding common selection methods. Some natural aaRSs have detectable activity for the ncAA of interest, precluding effective counterselection of the original AA activity by common methods. Thus, directed evolution has never been used to obtain aaRSs that were active towards nonstandard backbones.

Computer simulations that mimic directed evolution are another route, through computational protein design (CPD). Thus, tyrosyl-tRNA synthetase (TyrRS) was engineered recently to prefer the substrate D-Tyr over L-Tyr [13], using CPD to suggest mutations that were then tested experimentally. Recently, we engineered MetRS by CPD to obtain new variants with activity for adenylate formation by the native substrate  $\alpha$ -Met, as a proof of principle [14]. Here, we turn to  $\beta$ -Met, an ncAA with a nonstandard backbone. We report the redesign of MetRS to decrease its preference for  $\alpha$ -Met over  $\beta$ -Met, using a combination of CPD and experiments. The CPD calculations used a novel adaptive landscape flattening method [15, 16], which allows protein variants to be sampled according to their substrate binding affinity. A straightforward extension samples according to the binding free energy difference between two substrates [14, 16], such as  $\alpha$ -Met and  $\beta$ -Met. This contrasts with most

previous CPD work, where enzyme mutations were sampled according to the total energy of the enzyme-substrate complex [12, 13, 17–20].

To sample mutations that enhance ligand binding, we first flatten the free energy landscape of the apo enzyme in sequence space, using an adaptive, Wang-Landau Monte Carlo (MC) procedure to optimize a bias function that depends on sequence [15, 21]. The optimized bias approximates the free energy of the apo system, as a function of sequence, with its sign changed. Next, we simulate the protein–ligand complex, including the bias, which “subtracts out” the apo state. Remarkably, protein variants are then populated according to the apo/holo free energy difference, which is the binding free energy. Thus, the new method selects variants directly for substrate binding, and tight binders are exponentially enriched over the course of the MC trajectory. A straightforward extension allows us to sample for the  $\alpha$ -Met/ $\beta$ -Met binding free energy difference, or specificity. The new methods were successful in the previous MetRS redesign [14], and we expected they would yield more hits and fewer false positives in the present application, compared to the older methods that considered the total energy [12, 13, 17–19].

Three positions close to the  $\beta$ -Met substrate were chosen for design. The CPD procedure sampled several thousand sequence variants. 18 predicted hits were tested, 10 of which exhibited detectable activity for  $\beta$ -MetAMP formation. The top four were characterized experimentally in considerable detail. The reactions of  $\alpha$ -Met and  $\beta$ -Met with ATP to form the aminoacyl adenylates  $\alpha$ -MetAMP and  $\beta$ -MetAMP were characterized by their catalytic efficiencies—the ratio between the rate constant for the catalytic step,  $k_{\text{cat}}$ , and the Michaelis constant,  $K_M$ . Dissociation constants, catalytic rates, and Michaelis constants for both  $\alpha$ -Met and  $\beta$ -Met were measured. The best mutant retained a preference for  $\alpha$ -Met over  $\beta$ -Met; however, the preference was reduced compared to the wildtype by a factor of 29. For this and one other mutant, high resolution crystal structures were obtained, both alone and in complex with  $\beta$ -Met. The increase in relative  $\beta$ -Met activity should considerably facilitate its further optimization using experimental directed evolution, once an effective selective pressure has been established. Indeed, directed evolution is more likely to succeed if the starting activity level ( $\beta$ -Met vs.  $\alpha$ -Met) is not too low. More generally, the new method should facilitate the redesign of aaRSs and enzymes in general, and help expand the genetic

code to include nonstandard backbone chemistries.

## Materials and methods

### Designing for ligand binding

The protein is modeled with molecular mechanics, with a fixed backbone and a discrete rotamer library for side chains, while the solvent is modeled implicitly (see below). We perform a MC exploration of the protein [16] with either no ligand (apo state), or a ligand, say L (holo state). We gradually increment a bias potential until all the side chain types at the mutating positions have roughly equal populations, thus flattening the free energy landscape. We number the mutating positions arbitrarily 1, ...,  $p$ . The bias  $E^B$  at time  $t$  has the form:

$$E^B(s_1(t), s_2(t), \dots, s_p(t); t) = \sum_i E_i^B(s_i(t); t) + \sum_{i < j} E_{ij}^B(s_i(t), s_j(t); t) \quad (1)$$

Here,  $s_i(t)$  represents the side chain type at position  $i$ . The first sum is over single amino acid positions; the second is over pairs. The individual terms are updated at regular intervals of length  $T$ . At each update, whichever sequence variant  $(s_1(t), s_2(t), \dots, s_p(t))$  is populated is penalized by adding an increment  $e_i^B(s_i(t); t)$  or  $e_{ij}^B(s_i(t), s_j(t); t)$  to each corresponding term in the bias. The increments have the form:

$$e_i^B(s_i(t); t) = e_0 \exp[-E_i^B(s_i(t); t)/E_0] \quad (2)$$

$$e_{ij}^B(s_i(t), s_j(t); t) = e_0 \exp[-E_{ij}^B(s_i(t), s_j(t); t)/E_0] \quad (3)$$

where  $e_0$  and  $E_0$  are constant energies. Over time, the bias for the most probable states grows until it pushes the system into other regions of sequence space.

The sampled population of a sequence  $S$  is normalized to give a probability, denoted  $\tilde{p}_X(S)$ , where  $X$  indicates which protein state is considered, apo or holo. The probability can be converted into a free energy  $\tilde{G}_X$ :

$$\begin{aligned} \tilde{p}_X(S) &= \frac{1}{Z_X} \exp(-\tilde{G}_X(S)/kT) \\ \tilde{G}_X(S) &= -kT \ln \tilde{p}_X(S) - kT \ln Z_X \end{aligned} \quad (4)$$

where  $Z_X$  is a normalization factor that depends on  $X$  but not  $S$ . We also have a  
relation between the free energies with and without the bias:

$$\tilde{G}_X(S) = G_X(S) + E^B(S) \quad (5)$$

In practice, we will flatten the landscape not only of the apo state, but also the  
landscapes in the presence of the wildtype ligand and the new ligand targeted by the  
design. We will then take free energy differences between the three states, to obtain  
binding free energies and free energy differences between sampled sequences.

## Energy function and matrix

The energy was computed using an MMGBLK (molecular mechanics + Generalized  
Born + Surface Area or Lazaridis-Karplus):

$$E = E_{\text{MM}} + E_{\text{GB}} + E_{\text{LK}} \quad (6)$$

The MM term used the Amber ff99SB force field [22]. The GB term and its  
parametrization were described earlier [23]; similarly for the LK term [24]. The GB  
term used a “Fluctuating Dielectric Boundary” (FDB) method, where the GB  
interaction between two residues  $I, J$  was expressed as a polynomial function of their  
solvation radii [25]. These were kept up to date over the course of the MC simulation,  
so the GB interaction could be deduced on-the-fly with little additional calculation [25].  
The solvent dielectric constant was 80; the protein dielectric was 6.8 [24].

To allow very fast MC simulations, we precomputed an energy matrix for each  
system [26,27]. For each pair of residues  $I, J$  and all their allowed types and rotamers,  
we performed a short energy minimization (15 conjugate gradient steps) [16,25]. The  
backbone was fixed (in its crystal geometry) and the energy only included interactions  
between the two side chains and with the backbone. At the end of the minimization, we  
computed the interaction energy between the two side chains. Side chain–backbone  
interaction energies were computed similarly (and formed the matrix diagonal).

## Structural models

115

### MetRS complexes

116

Several MetRS complexes were modeled earlier and used here. For MetRS–ATP [14], we started from a crystal complex (PDB code 1PG0) between *E. coli* MetRS and a methionyl adenylate (MetAMP) analogue [28] with the KMSKS loop in its inactive conformation. Next, 15 loop residues from the the active loop conformation were transplanted from the *Leishmania major* structure (PDB code 3KFL) [29] by aligning common ligand fragments in both structures. Several loop residues were mutated into the *E. coli* types with Scwrl4 [30]. We adjusted the model geometry using 40 steps of conjugate gradient minimization to obtain a model of *E. coli* MetRS with the KMSKS loop in the active conformation. Finally, adenylate and pyrophosphate fragments were used to align ATP in the binding site. A Mg<sup>2+</sup> ion was already in the 3KFL structure and was transferred to the new model. We call this model the MetRS–ATP complex.  $\alpha$ -Met was added to form a MetRS–Met–ATP complex. Similarly, MetAMP was added, by superimposing it on the analogue present in 1PG0.

117

118

119

120

121

122

123

124

125

126

127

128

129

Recently [16], we added  $\beta$ -Met to MetRS–ATP. We used the recent crystal structure (PDB code 6SPN) of a complex between *E. coli* MetRS and  $\beta$ -Met [31]. We aligned that structure to MetRS–ATP to form MetRS– $\beta$ -Met–ATP. The 6SPN crystal structure included two conformations for the  $\beta$ -Met carboxylate. One is much closer to the ATP, as required for catalysis, and we chose that geometry. Complexes with the activated substrates [ $\alpha$ -MetATP]<sup>‡</sup> and [ $\beta$ -Met–ATP]<sup>‡</sup> were built earlier [14, 16], using a restrained minimization to produce the appropriate pentavalent geometry around the ATP  $\alpha$  phosphorus. Here, we also formed the complex with  $\beta$ -MetAMP, by superimposing the latter onto MetAMP in the MetRS–MetAMP complex. The complex with  $\beta$ -ValAMP was constructed by replacing the amino acid moiety.

130

131

132

133

134

135

136

137

138

139

For each complex, the geometry of the protein around the ligands was relaxed slightly by performing a short, restrained molecular dynamics simulation, with the ligands held fixed. The entire system was placed in a large box of explicit TIP3P water [32]. Harmonic restraints were applied to nonhydrogen atoms, with force constants that decreased gradually from 5 to 0.5 kcal/mol/Å<sup>2</sup> over 575 ps of dynamics, performed with the NAMD program [33]. The final protein geometry was used for the

140

141

142

143

144

145



design calculations. We have found that this procedure reduces specialization of the backbone model towards each particular ligand.

For the design calculations, the protein backbone and side chains more than 20 Å from the ligand were held fixed. The other side chains were allowed to explore rotamers, taken from the Tuffery library, augmented to allow multiple orientations for certain hydrogen atoms [16, 34]. For  $\alpha$ -Met and  $\beta$ -Met, we allowed the Met rotamers from the Tuffery library, with the rest of the ligand held fixed. Side chains 13, 256 and 297 were allowed to mutate into all types except Gly and Pro. Thus, there were 5832 possible sequences in all. Histidine protonation states at non-mutating positions were assigned by visual inspection of the 3D structure. System preparation was done using the protX module of the Proteus design software [35].

### Unfolded state

The unfolded state energy was estimated with a tri-peptide model [36]. For each mutating position, side chain type, and rotamer, we computed the interaction between the side chain and the tri-peptide it forms with the two adjacent backbone and  $C_{\beta}$  groups. Then, for each allowed type, we computed the energy of the best rotamer and averaged over mutating positions. The mean energy for each type was taken to be its contribution to the unfolded state energy. The contributions of the mutating positions were summed to give the total unfolded energy.

### Ligand force field

The partial charges of ribose, adenine and side chain fragments were derived from existing Amber parameters in analogous fragments. For the junction atoms between  $\beta$ -Met and AMP, we performed an HF/6-31G\* ab initio calculation with Gaussian 9, and partial charges were chosen to reproduce the electrostatic potential, following the usual Amber procedure [22]. Bonded and van der Waals parameters were assigned by analogy to the  $\alpha$ -Met model [14]. Parameters for the implicit solvent energy terms were assigned by analogy to existing groups. The Mg charge was set to +1.5, as previously [14].

## Monte Carlo simulations

174

To optimize the bias potential, we performed MC simulations of the considered state  
with bias updates every  $T = 1000$  steps, with  $e_0 = 0.2$  kcal/mol and  $E_0 = 50$   
kcal/mol [15]. During the first  $10^8$  MC steps, we optimized a bias potential including  
only single-position terms. There were  $p = 3$  mutating positions, which all contributed  
to the bias. In the second stage, we ran MC simulations of  $5.10^8$  MC steps [16], using 8  
replicas with thermal energies (kcal/mol) of 0.17, 0.26, 0.39, 0.59, 0.88, 1.33, 2.0 and 3.0.  
Temperature swaps were attempted every 500 steps. All the replicas experienced the  
same bias potential. Both stages used 1- and 2-position moves.

175

176

177

178

179

180

181

182

## Experimental mutagenesis and kinetic assays

183

### Purification of wildtype and mutant MetRS

184

Throughout this study, we used a His-tagged M547 monomeric version of *E. coli* MetRS,  
fully active, both *in vitro* and *in vivo* [37]. The gene encoding M547 MetRS from  
pBSM547+ [38, 39] was subcloned into pET15b[*lpa*] [40] to overproduce the His-tagged  
enzyme in *E. coli* [31]. Site-directed mutations were generated using the QuikChange  
method [41], and the whole mutated genes verified by DNA sequencing. The enzyme  
and its variants were produced in BLR(DE3) *E. coli* cells. Transformed cells were grown  
overnight at 37°C in 0.25 L of TBAI autoinducible medium containing 50 µg/ml  
ampicillin. They were harvested by centrifugation and resuspended in 20 ml of buffer A  
(10 mM Hepes-HCl pH 7.0, 3 mM 2-mercaptoethanol, 500 mM NaCl). They were  
disrupted by sonication (5 min, 0°C), and debris was removed by centrifugation (15,300  
G, 15 min). The supernatant was applied on a Talon affinity column (10 ml; Clontech)  
equilibrated in buffer A. The column was washed with buffer A plus 10 mM imidazole  
and eluted with 125 mM imidazole in buffer A. Fractions containing tagged MetRS were  
pooled and diluted ten-fold in 10 mM Hepes-HCl pH 7.0, 10 mM 2-mercaptoethanol  
(buffer B). These solutions were applied on a Q Hiload ion exchange column (16 mL,  
GE-Healthcare), equilibrated in buffer B containing 50 mM NaCl. The column was  
washed with buffer B and eluted with a linear gradient from 5 to 500 mM NaCl in  
buffer B (2 ml/min, 10 mM/min). Fractions containing tagged MetRS were pooled,  
dialyzed against a 10 mM Hepes-HCl buffer (pH 7.0) containing 55% glycerol, and

185

186

187

188

189

190

191

192

193

194

195

196

197

198

199

200

201

202

203

stored at -20°C. The MetRS was estimated by SDS-PAGE to be at least 95% pure. 204

### Measurement of ATP-PPi isotopic exchange activity 205

Prior to activity measurements, MetRS was diluted in standard buffer (20 mM Tris-HCl 206  
buffer pH 7.6, 10 mM 2-mercaptoethanol, 0.1 mM EDTA) containing 0.2 mg/ml bovine 207  
serum albumin (Aldrich) if the concentration after dilution was less than 1  $\mu$ M. Initial 208  
rates of ATP-PPi exchange activity were measured at 25°C as described [42]. In brief, 209  
the 100  $\mu$ l reaction mixture contained Tris-HCl (20 mM, pH 7.6), MgCl<sub>2</sub> (7 mM), ATP 210  
(2 mM), [<sup>32</sup>P]PPi (1800-3700 Bq, 2 mM) and various concentrations (0-16 mM) of the 211  
Met amino acid. The exchange reaction (Fig 1) was started by adding catalytic 212  
amounts of MetRS (20  $\mu$ l). After quenching the reaction, <sup>32</sup>P-labeled ATP was 213  
adsorbed on charcoal, filtered, and measured by scintillation counting. For 214  
 $\beta$ -Val-dependent activity measurements,  $\alpha$ -Met was replaced by 10 mM  $\beta$ -Val. In this 215  
case, all reaction components were treated with MGL to remove contaminating  $\alpha$ -Met. 216

### Measurement of ATP-PPi exchange activity 217

Prior to activity measurements, MetRS or its variants were diluted in standard buffer 218  
(20 mM Tris-HCl buffer pH 7.6, 10 mM 2-mercaptoethanol, 0.1 mM EDTA) containing 219  
0.2 mg/ml bovine serum albumin (Aldrich) if the concentration after dilution was less 220  
than 1  $\mu$ M. Initial rates of ATP-PPi exchange activity were measured at 25°C as 221  
described [31]. In brief, the 100  $\mu$ l reaction mixture contained Tris-HCl (20 mM, pH 222  
7.6), MgCl<sub>2</sub> (7 mM), ATP (2 mM), [<sup>32</sup>P]PPi (1800-3700 Bq, 2 mM) and various 223  
concentrations of  $\alpha$ -Met. The exchange reaction (Fig 1) was started by adding catalytic 224  
amounts of MetRS (20  $\mu$ l). After quenching the reaction, <sup>32</sup>P-labeled ATP was 225  
adsorbed on charcoal, filtered, and measured by scintillation counting. For 226  
 $\beta$ -Val-dependent activity measurements,  $\alpha$ -Met was replaced by 10mM  $\beta$ -Val. In this 227  
case, all reaction components were treated with MGL to remove contaminating  $\alpha$ -Met. 228

### Fluorescence at equilibrium 229

Variations of the intrinsic fluorescence of M547 and its variants (0.5  $\mu$ M) upon titration 230  
with substrates were followed at 25°C in 20 mM Tris-HCl (pH7.6), 10 mM 231  
2-mercaptoethanol, 2 mM MgCl<sub>2</sub> and 0.1mM EDTA as described [31, 42, 43]. 232

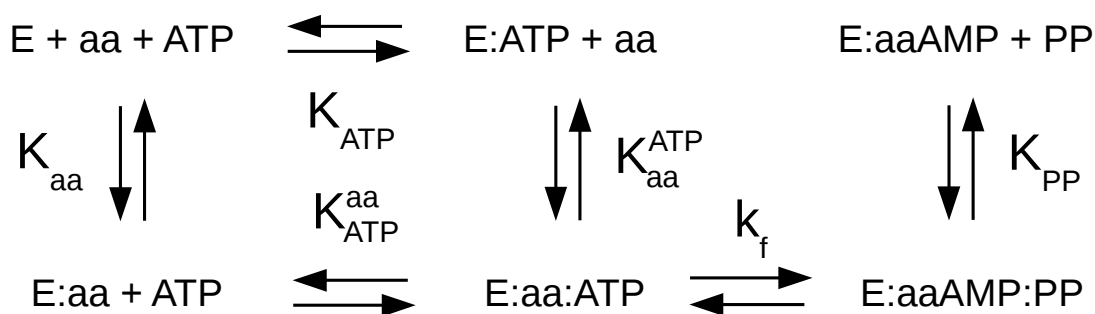
Measurements were done in a Hellma 1 cm × 0.4 cm cuvette with an FP-8300 JASCO 233  
spectrofluorometer (295 nm excitation, 340 nm emission). All titration curves were 234  
corrected for dilution. Concentrations of  $\alpha$ -Met or  $\beta$ -Met were varied from 3  $\mu$ M to 1 235  
mM and from 0.06 mM to 4 mM, respectively. Data were fitted to simple saturation 236  
curves from which the corresponding dissociation constants were derived using the 237  
Origin software (OriginLab Corp.). 238

### Fluorescence at the pre-steady state 239

Fluorescence measurements at the pre-steady-state were performed as 240  
described [31,42,44] using an SX20 stopped flow apparatus (Applied Photophysics, UK). 241  
All experiments were performed in standard buffer supplemented with 2 mM MgCl<sub>2</sub>. 242  
The formation of  $\alpha$ - or  $\beta$ -methionyl adenylate was initiated by mixing 1:1 (v/v) an 243  
enzyme solution (1  $\mu$ M for  $\alpha$ -Met or 2  $\mu$ M for  $\beta$ -Met) containing ATP-Mg<sup>2+</sup> (2 mM) 244  
and PPi (10  $\mu$ M) with a solution containing the same concentrations of ATP-Mg<sup>2+</sup> plus 245  
variable amounts of the amino acid (10  $\mu$ M to 640  $\mu$ M for  $\alpha$ -Met or 25  $\mu$ M to 2 mM for 246  
 $\beta$ -Met). After mixing, fluorescence was recorded and fitted to single exponentials from 247  
which the rate constants were derived. Each rate was determined three times. Kinetic 248  
( $k_f(\text{aa})$ ) and equilibrium ( $K_{\text{aa}}^{\text{ATP}}$ ) parameters are defined in Fig 1. They were deduced 249  
from the fit of the measured rate constants to the theoretical saturation curves [42–44] 250  
using Origin. Each experiment was performed at least twice independently. Results 251  
below are expressed as mean  $\pm$  either standard deviation from the independent 252  
experiments or standard error from the fitting procedure, whichever is greater. All 253  
experiments were performed using MGL-treated  $\beta$ -Met. 254

### X-ray structure determination 255

Crystals of the MetRS CAC and MAC variants were obtained by microseeding with 256  
crystals of M547 [45] in a solution containing 30 mM KPO<sub>4</sub>, 4 mM 2-mercaptoethanol, 257  
1.08 mM ammonium citrate (pH 7.0) and 3.6 mg/mL of protein. Type 2 crystals [37] of 258  
the apo-CAC and -MAC enzymes were chosen. For the structures of MetRS: $\beta$ -Met 259  
complexes, 10 mM  $\beta$ -Met and 1 mM adenosine were added to the crystallization 260  
medium prior to microseeding. Before data collection, crystals were quickly soaked in a 261



**Fig 1. MetRS reactions to form aminoacyl adenylate.** The amino acid is denoted aa and the enzyme E. Equilibrium constants are in uppercase;  $k_f$  is a rate constant.

solution containing 1.4 M ammonium citrate, 30 mM potassium phosphate (pH 7.0) and 25% v/v of glycerol and flash-cooled in liquid nitrogen. In the case of MetRS: $\beta$ -Met complexes, the cryoprotecting solution was supplemented with 10 mM  $\beta$ -Met. Data were collected at the Proxima 2 beamline at the SOLEIL synchrotron (Gif sur Yvette, France). Diffraction images were analyzed with the XDS program [46] and the data further processed using programs from the CCP4 package [47]. The structure was solved by rigid body refinement of the wild-type MetRS model (PDB id 3H9C) [37], using PHENIX [48]. Coordinates and associated B factors were refined through several cycles of manual adjustments with Coot [49] and positional refinement with PHENIX. For MetRS: $\beta$ -Met structures, no bound adenosine was observed. Data collection and refinement statistics are summarized in Supplementary Table SM1. Attempts to obtain the structures of the two variants bound to  $\alpha$ -Met only revealed a very low occupancy of the amino acid binding site and were not analyzed further.

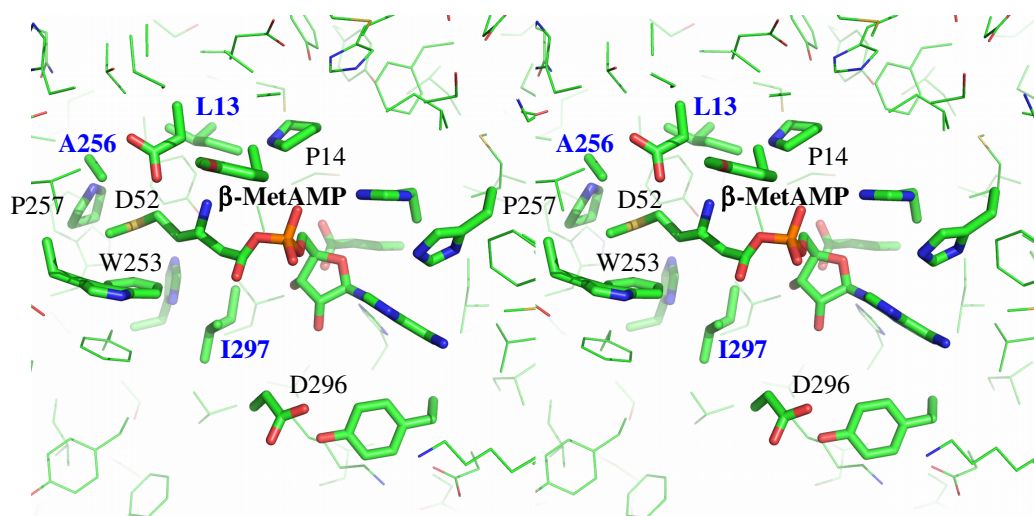
## Results

### Computational design of MetRS to bind $\beta$ -MetAMP and $\beta$ -ValAMP

MetRS was redesigned through adaptive MC simulations where three active site positions, 13, 256, 297 (Fig 2) were allowed to mutate freely. With  $\beta$ -MetAMP binding as the design target, adaptive landscape flattening was applied to the apo state. In practice, over the course of a long MC simulation, the bias was gradually optimized,

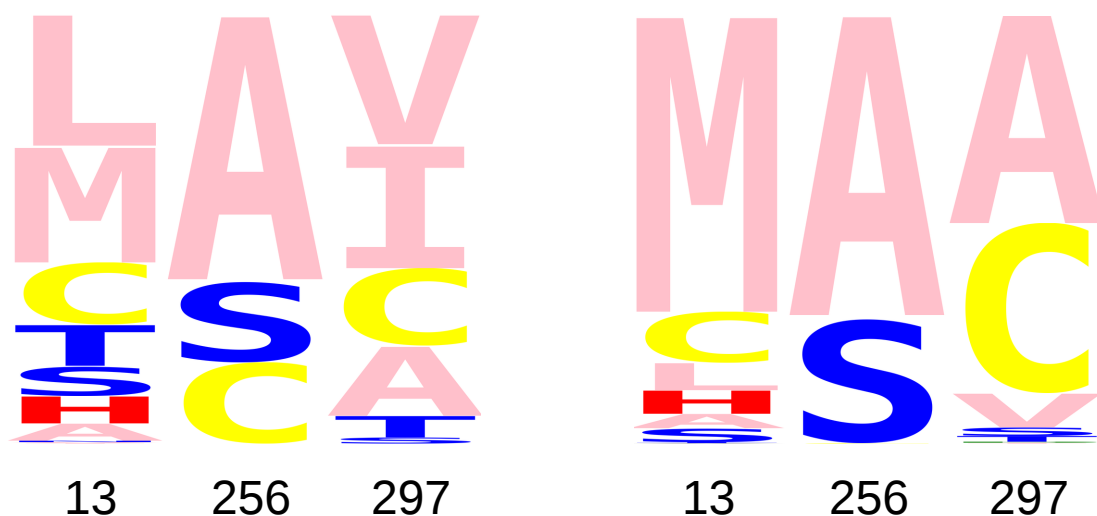
until the free energy landscape was sufficiently flattened (all amino acid types were 282  
sampled at all three positions with roughly equal populations) [15]. Then, a second 283  
simulation was done, of the holo state, with the bias included. Sequences sampled with 284  
either  $\alpha$ -MetAMP or  $\beta$ -MetAMP as the ligand are shown in Fig 3, as logos. With the 285  
 $\alpha$ -Met ligand, the wildtype amino acid types, L, A, I were highly ranked at all three 286  
designed positions. 287

With  $\beta$ -Met binding as the design criterion, the wildtype variant LAI was not 288  
sampled in the holo state. However, the similar variants LSI, MAI and LAA were 289  
sampled. Their predicted binding free energies were within 0.5 kcal/mol of each other 290  
and can be taken as points of reference. 35 variants were predicted to have  $\beta$ -MetAMP 291  
binding that was improved, compared to LSI. 25 were improved by 0.5 kcal/mol or 292  
more. The maximum improvement was 3.6 kcal/mol. The predominant amino acid 293  
types (Fig 3, right) were MCL at position 13, AS at position 256, and ACV at position 294  
297. The top 10 predictions are listed in Table 1. Several predicted variants were active, 295  
as detailed in the next section.



**Fig 2. Stereo view of the wildtype MetRS binding pocket, showing  $\beta$ -MetAMP and selected side chains.**

Redesign for  $\beta$ -Val activity was unsuccessful. We targeted  $\beta$ -ValAMP binding, 297  
varying the same three positions. The top 8 predictions are included in Table 1. In the 298



**Fig 3. Designed sequence logos.** **Left)** MetRS sequences sampled according to their predicted  $\alpha$ -MetAMP binding free energies. The three mutating positions, 13, 256, 297 are shown. The height of each letter measures the frequency of its type, when the sampled sequences are weighted by their ligand binding free energies. **Right)** MetRS sequences sampled according to their predicted  $\beta$ -MetAMP binding free energies.

**Table 1.** Predicted  $\beta$ -MetAMP and  $\beta$ -ValAMP binding affinities for top MetRS redesigns

seq. <sup>a</sup>	fold <sup>b</sup>	$\beta$ -MetAMP		seq. <sup>a</sup>	fold <sup>b</sup>	$\beta$ -ValAMP		
			binding				binding	rank <sup>c</sup>
MAA	2.0		-3.5	MAC	2.3		-6.3	1
MAC	2.3		-3.4	CAC	-7.9		-4.2	2
MAV	1.3		-2.4	SAC	-4.0		-4.1	3
CSA	-6.3		-2.2	LAC	-0.3		-3.8	4
HSA	2.7		-2.1	AAC	-7.8		-3.3	5
CSC	-6.2		-2.1	HAC	0.4		-2.7	6
LSC	1.2		-2.1	MAV	1.3		-2.7	7
LSA	1.0		-2.0	CAT	-5.6		-2.5	8
SSA	-2.5		-1.8	CAV	-8.8		-0.6	25
ASA	-5.9		-1.8	LAV	-1.3		0.6	38

<sup>a</sup>Sequence at the designed positions 13, 256, 297, ranked by  $\beta$ -MetAMP or  $\beta$ -ValAMP binding free energies (kcal/mol) relative to the reference LSI ( $\beta$ -Met) or LAI (wildtype;  $\beta$ -Val). <sup>b</sup>Estimated folding free energy, relative to the reference sequence. <sup>c</sup>Rank according to  $\beta$ -ValAMP binding.

top variants, the native A was predominant at position 256, while position 297 strongly preferred C and position 13 was more variable. Experimental tests were done for four mutants: CAC and LAC, among the top predictions, and CAV and LAV, which were ranked somewhat lower. No  $\beta$ -Val-dependent ATP-PPi isotopic exchange activity was detected.

## Experimental characterization of four variants designed for

### $\beta$ -Met activity

From the 35 top predicted variants, 18 were chosen for experimental testing, such that they recapitulated the predominant amino acid types predicted at each redesigned position. They were tested for  $\beta$ -MetAMP synthesis using the pre-steady state fluorescence assay in the presence of 2 mM ATP-Mg<sup>2+</sup> and 10 mM  $\beta$ -Met. All reaction components were extensively treated with MGL, to remove any contaminating  $\alpha$ -Met. 10 of the 18 variants were active, albeit with a reduced, not an increased activity compared to the wildtype. Variants that included an A256S mutation were all inactive. The others all preserved the native Ala256, associated with A, C, V, or native I at position 297 and M, C, L or S at position 13. Details and experimental kinetic parameters are reported in Supplementary Table SM2. Below, we report a detailed characterization of the four best experimental variants: MAC, CAC, SAC, and LAC, which are all compared to the wildtype LAI. “Best” variants were chosen for their relative  $\alpha$ -Met and  $\beta$ -Met activities, reported in Table SM2.

**Table 2.** Experimental parameters for top MetRS redesigns

	LAI (WT)	MAC	CAC	SAC	LAC
$K_d(\alpha\text{-Met})$ (mM)	0.050(5) <sup>c</sup>	0.16(2)	0.17(3)	0.17(2)	0.19(3)
$K_{\alpha\text{-Met}}^{\text{ATP}}$ (mM)	0.070(4)	1.1(2)	>5	>5	1.3(1)
$k_f(\alpha\text{-Met})$ (s <sup>-1</sup> )	260±10	33.9±1.9	NA	NA	139±17
$k_f(\alpha\text{-Met})/K_{\alpha\text{-Met}}^{\text{ATP}}$ (s <sup>-1</sup> mM <sup>-1</sup> )	3714±143	31.5±4.4	14.7±0.1	17.9±1.5	107±2
aminoacylation rate <sup>a</sup> (s <sup>-1</sup> )	1.9(2)	0.017(4)	0.013(2)	0.016(3)	0.07(1)
$K_d(\beta\text{-Met})$ (mM)	1.2(2)	0.9(3)	0.9(2)	1.0(3)	0.9(3)
$K_{\beta\text{-Met}}^{\text{ATP}}$ (mM)	0.26	0.58	0.56	1.3	0.26
$k_f(\beta\text{-Met})$ (s <sup>-1</sup> )	0.047(4)	0.0083(3)	0.0105(8)	0.007(1)	0.013(1)
$k_f(\beta\text{-Met})/K_{\beta\text{-Met}}^{\text{ATP}}$ (s <sup>-1</sup> mM <sup>-1</sup> )	0.180(4)	0.015(3)	0.021(8)	0.0054(12)	0.05(1)
$10^4 \times \beta\text{-Met}/\alpha\text{-Met}$ ratio <sup>b</sup>	0.5	5.0	14.0	3.0	5.0
$\beta$ -Met enhancement	1	10	29	6	10

Experimental enzyme parameters. <sup>a</sup>Initial rate for tRNA acylation with  $\alpha$ -Met, measured as reported earlier [31]. <sup>b</sup> $k_f(\text{aa})/K_{\text{aa}}^{\text{ATP}}$  ratio. <sup>c</sup>In parentheses: experimental uncertainty in significant digits.

### Selected mutations at positions 13 and 297 strongly affect MetAMP formation

The enzyme reaction constants are defined in Fig 1. Experimental values are reported in Table 2. The  $\alpha$ -Met dissociation constants  $K_d$  of the mutants were increased 3-4 fold, based on steady-state fluorescence measurements. With ATP present, the  $\alpha$ -Met dissociation constants  $K_{\alpha\text{-Met}}^{\text{ATP}}$  were increased more strongly, by factors of 15 and 19 for



MAC and LAC, and by factors of 30 for CAC and SAC, based on the fluorescence at 325  
the pre-steady state. We also derived the rate constants  $k_f$  for  $\alpha$ -Met activation. The 326  
rates were decreased by an order of magnitude for MAC and by a factor of 2 for LAC. 327  
For CAC and SAC, the rates could not be measured, as  $K_{\alpha\text{-Met}}^{\text{ATP}}$  was too large. Catalytic 328  
efficiencies  $k_f(\alpha\text{-Met})/K_{\alpha\text{-Met}}^{\text{ATP}}$  for  $\alpha$ -Met activation were reduced by two orders of 329  
magnitude for MAC, CAC and SAC, and by a factor of more than 30 for LAC. Note 330  
that this parameter directly reflects the free energy difference between the transition 331  
state complex and the E:ATP:Mg<sup>2+</sup> +  $\alpha$ -Met state. These reduced efficiencies for the 332  
activation reaction are also reflected in the off rates of the global aminoacylation 333  
reaction, which were reduced in similar proportions. Overall, the  $\alpha$ -Met catalytic 334  
efficiencies were reduced (transition state binding was weakened) and the mutations at 335  
both positions (13 and 297) contributed (the single mutant LAC was more active than 336  
the double mutants). Reduction was largest for the CAC and SAC variants (Table 2). 337

#### **Activation of $\beta$ -Met is much less affected than that of $\alpha$ -Met**

 338

The  $\beta$ -Met used throughout was treated enzymatically to remove any contaminating 339  
 $\alpha$ -Met. The enzyme employed was a bacterial methionine  $\gamma$ -lyase, which breaks down 340  
 $\alpha$ -Met but not  $\beta$ -Met [31]. From steady-state fluorescence measurements, the  $\beta$ -Met 341  
dissociation constants of the mutants were only slightly reduced, compared to wildtype 342  
MetRS (25% decrease; Table 2). On the other hand, with ATP present, pre-steady-state 343  
fluorescence showed that the dissociation constants  $K_{\beta\text{-Met}}^{\text{ATP}}$  were unaffected in LAC, 344  
increased by a factor of 2 in MAC and SAC, and by a factor of 5 in SAC. The rates 345  
 $k_f(\beta\text{-Met})$  of  $\beta$ -Met activation were decreased by factors ranging from 4 (LAC) to 7 346  
(SAC). The catalytic efficiency was reduced by a factor of 3.6 for the single mutant 347  
(LAC). For the double mutants, the lowering of the catalytic efficiency was greatest for 348  
CAC (8.6 fold). In all cases, activation of  $\beta$ -Met was less affected than that of  $\alpha$ -Met. 349  
As a result, the selectivity of all four mutant enzymes for  $\beta$ -Met vs.  $\alpha$ -Met was 350  
increased. For SAC, LAC and MAC, the increase was between 6 and 10. For the double 351  
mutant CAC, the  $\beta$ -Met vs.  $\alpha$ -Met selectivity was increased 29-fold. 352

## Crystal structures of the CAC and MAC variants

The structures of the CAC and MAC variants were solved in both the apo and  $\beta$ -Met bound forms. The apo structures did not show any significant conformational changes compared to the wild-type enzyme (Supplementary Figure SM1 A-B). The substituted residues, C13 and C297 (CAC), or M13 and C297 (MAC) were clearly visible in the electron density. Additional electron density close to the sulfur atom of C297 was visible in both structures. We modelled this density as a water molecule, which refined at a distance from the sulfur atom of 2.6 Å (CAC) or 2.3 Å (MAC; Supplementary Figure SM1 C-D). Although the density was best accounted for by a Cys and a water molecule, it cannot be excluded that a fraction of C297 residues in the crystal have been oxidized to sulfenic acid. Indeed, X-ray induced oxidation of Cys has already been observed and proposed to require a reactive cysteine near a water molecule [50].

For both holo structures,  $\beta$ -Met was clearly visible in the active site. In wild-type MetRS, binding of  $\beta$ -Met and  $\alpha$ -Met, both occur via a ligand-induced, concerted rearrangement of aromatic side chains (W229, W253, F300 and F304) [31] that puts W253 in contact with the Met side chain. This rearrangement did not fully occur with the present MetRS variants upon  $\beta$ -Met binding. With CAC, F300 and F304 remained in their apo positions whereas a minor fraction of W229 was rotated (Supplementary Figure SM2). W253 mainly rotated to a position that differs from that in wild-type MetRS: $\beta$ -Met. With MAC, the rearrangement was closer to that observed in the wild-type enzyme. W253 and F304 mainly rotated to the same position as in the wild-type MetRS: $\beta$ -Met complex, but only minor fractions of W229 and F300 moved away from their apo positions. These partial rearrangements in the CAC and MAC variants probably contribute to the observed loss of catalytic efficiency towards both  $\alpha$ -Met and  $\beta$ -Met (Table 2).

In the wild-type MetRS: $\alpha$ -Met complex, the concerted rearrangement of aromatic residues is accompanied by a rotation of Y15 side chain that places the  $\alpha$ -Met carboxylate in its active position (position 1), favorable to catalysis [28, 37, 51]. In the  $\beta$ -Met complex, the rotated position of Y15 was unstable and several alternative conformations were observed [31]. Concomitantly, two alternative positions of the  $\beta$ -Met carboxylate were observed. In the major conformation (position 2), the carboxylate

pointed away from the active site, preventing the full rotation of Y15. In the minor 384  
conformation (position 3), the carboxylate was closer to the active state seen with 385  
 $\alpha$ -Met (position 1). 386

With the CAC variant, the  $\beta$ -Met carboxylate mainly adopted a position (position 4) 387  
closer to position 1 than position 3 (Supplementary Fig SM1 E). Consistent with this, 388  
the locking conformation of Y15 was more highly occupied (Supplementary Fig SM2 389  
A-B and D). Thus, in the CAC variant, the  $\beta$ -Met carboxylate is mainly in a position 390  
favorable to catalysis. This might account for the increased selectivity of this variant 391  
towards  $\beta$ -Met. With the MAC variant, in contrast, only position 2 of the  $\beta$ -Met 392  
carboxylate was visible (Supplementary Fig SM2 C). 393

The CAC and MAC variants both had a carbon at position 297 of the amino acid 394  
binding pocket. As mentioned above, C297 tightly bound a water molecule that was 4.5 395  
 $\text{\AA}$  away from the  $\beta$ -Met sulphur atom. This likely contributes to  $\beta$ -Met/ $\alpha$ -Met binding. 396  
Interestingly, in the CAC variant, the C297 sulphur atom was 4.5  $\text{\AA}$  away from the 397  
 $\beta$ -Met carboxylate (Supplementary Fig SM2 A). Thus, C297 may favor the activation of 398  
 $\beta$ -Met more than that of  $\alpha$ -Met. 399

In the CAC variant and the wild-type enzyme, the main chain oxygen of residue 13 400  
interacted with the amino group of  $\beta$ -Met and the Y15 main chain nitrogen interacted 401  
with a  $\beta$ -Met carboxylate oxygen (Supplementary Fig SM2 B,C). Because of the bulkier 402  
Met side chain at position 13, the MAC variant showed a slight displacement of the 403  
main chain (0.5  $\text{\AA}$  for the  $C_\alpha$  of residue 13). This displacement probably leads to subtle 404  
changes in the  $\beta$ -Met environment during catalysis. Overall, it appears that better 405  
positioning of the  $\beta$ -Met carboxylate and tuning of the conformation of the A12-Y15 406  
region are good ways to enhance the selectivity of MetRS for  $\beta$ -Met over  $\alpha$ -Met. 407

## Concluding discussion 408

Genetic code expansion for noncanonical backbones would open exciting new directions 409  
for protein engineering, allowing new structural motifs and building blocks. We envisage 410  
that ncAAs could be developed in two “orthogonal” directions, where a variety of 411  
noncanonical backbones could be combined with different noncanonical side chains, 412  
leading to a combinatorial space of ncAAs. Unfortunately, directed evolution of aaRSs 413

is still a major difficulty, and has never been used to obtain activity towards 414  
noncanonical backbones. One difficulty is that directed evolution requires not only a 415  
selective pressure, but also a starting enzyme that has a certain level of activity towards 416  
the ncAA. Natural MetRS enzymes do not provide this. 417

Here, we used a mixed computational and experimental approach. We searched for 418  
 $\beta$ -Met activity using CPD, then tested the predictions experimentally. CPD exploration 419  
used a powerful new adaptive sampling method. Indeed, most previous redesign studies 420  
of protein-ligand binding used the total system energy as the design target [20]. While 421  
many successes have been reported, the predicted designs often had a low activity, and 422  
many false positives were produced [11–13]. Here, instead of targeting the total energy, 423  
we used the new, adaptive sampling [14,15] to target ligand binding directly, applying 424  
positive design to the bound state and negative design to the unbound. 18 variants were 425  
selected for testing: 10 displayed detectable activity for  $\beta$ -Met. 426

The top four variants were characterized in detail experimentally. They had 427  
experimental preferences for  $\alpha$ -Met that were reduced, relative to  $\beta$ -Met, by factors of 6, 428  
10, 10, and 29. These reductions were due to reduced  $\alpha$ -Met activity, whereas the  $\beta$ -Met 429  
activities were close to the wildtype level. The high resolution X-ray structure of the 430  
best mutants, CAC and MAC, showed that the AA position was close to that used in 431  
the CPD calculations, and the active carboxylate moiety was positioned as expected to 432  
react with ATP. While the CPD calculations only considered the binding of  $\beta$ -Met 433  
adenylate, the top variants were also shown to aminoacylate cognate tRNA with  $\beta$ -Met. 434

Although the CPD calculations overestimated the strength of the redesigned  $\beta$ -Met 435  
binding, they did not produce any false positives for the three positions designed here. 436  
Additional calculations that targeted other positions did produce false positives, 437  
possibly because they considered positions that could affect the conformation of the 438  
flexible KMSKS loop in the active site [42]. Design for  $\beta$ -Val also produced false 439  
positives. This could be due to the use of an incorrect  $\beta$ -Val pose in the calculations; a 440  
more advanced study involving molecular dynamics (MD) and an explicit solvent model 441  
could be used to test this possibility. More sophisticated and expensive CPD procedures 442  
involving MD exploration of backbone degrees of freedom are another possibility [52, 53]. 443

The new methodology used here is applicable to many problems. For MetRS, it was 444  
used earlier to retrieve variants with azidonorleucine (Anl) activity [14]. The top 445

experimental variants were retrieved when the enzyme was redesigned for ligand binding 446  
*specificity* (AnI vs. Met), rather than AnI affinity. Specificity of transition state binding 447  
can also be targeted, in principle. The methodology was used here with a model where 448  
backbone flexibility was treated implicitly through a dielectric continuum model, 449  
implemented within the Proteus software [35]. However, the methodology is general and 450  
could be combined with other methods and software, such as lambda-dynamics with the 451  
Charmm software [52]. The successful design of MetRS variants with a large decrease in 452  
 $\alpha$ -Met activity, relative to  $\beta$ -Met, indicates that the assumptions used here are not too 453  
limiting, and that substrate binding affinity, as a design target, is a good proxy for 454  
activity. Experimental directed evolution is a future perspective, assuming an 455  
appropriate selective pressure for an extra backbone methylene can be identified. The 456  
best present design, with its 29-fold gain in relative  $\beta$ -Met activity, should be a valid 457  
starting point. 458

## Supporting information

459

**S1 Appendix.** **Additional data** are provided as a Supplementary Appendix, which provides statistics on X-ray data collection, experimental kinetic parameters for selected MetRS mutants, and 3D active site structure views for selected systems.

460

461

462

**S1 File.** **X-ray structures** are provided in four separate CIF files for the CAC and MAC mutants, determined with and without bound  $\beta$ -Met. The PDB identifiers are 8BRU (apo-MAC), 8BRV (MAC- $\beta$ -Met), 8BRW (apo-CAC), 8BRX (CAC- $\beta$ -Met).

463

464

465

## References

1. Ibba M, Francklyn C, Cusack S, editors. Aminoacyl-tRNA Synthetases. Landes Bioscience, Georgetown; 2005.
2. Xie J, Schultz PG. A chemical toolkit for proteins: an expanded genetic code. *Nat Rev Molec Cell Biol.* 2006;7:775–782.
3. Young TS, Schultz PG. Beyond the canonical twenty amino acids: expanding the genetic lexicon. *J Biol Chem.* 2010;285:11039–11044.
4. Liu CC, Schultz PG. Adding new chemistries to the genetic code. *Ann Rev Biochem.* 2010;79:413–444.
5. Neumann-Staubitz P, Neumann H. The use of unnatural amino acids to study and engineer protein function. *Curr Opin Struct Biol.* 2016;38:119–128.
6. Chin JW. Expanding and reprogramming the genetic code. *Nature.* 2017;550:53–60.
7. Wang L, Brock A, Herberich B, Schultz PG. Expanding the genetic code of *Escherichia coli*. *Science.* 2001;292:498–500.
8. Tanrikulu IC, Schmitt E, Mechulam Y, Goddard III W, Tirrell DA. Discovery of *Escherichia coli* methionyl-tRNA synthetase mutants for efficient labeling of proteins with azidonorleucine in vivo. *Proc Natl Acad Sci USA.* 2009;106:15285–15290.
9. Seebach D, Hook DF, Glättli A. Helices and other secondary structures of  $\beta$ - and  $\gamma$ -peptides. *Biopolymers.* 2006;84:23–37.
10. Wang P, Schepartz A.  $\beta$ -peptide bundles: design, build, analyze, biosynthesize. *Chem Comm.* 2016;52:7420–32.

11. Kuhn SM, Rubini M, Fuhrmann M, Theobald I, Skerra A. Engineering of an orthogonal aminoacyl-tRNA synthetase for efficient incorporation of the nonnatural amino acid O-methyl-L-tyrosine using fluorescence-based bacterial cell sorting. *J Mol Biol.* 2010;404:70–87.
12. Li R, Wijma HJ, Song L, Cui Y, Otzen M, Tian Y, et al. Computational redesign of enzymes for regio- and enantioselective hydroamination. *Nat Chem Biol.* 2018;14:664–670.
13. Simonson T, Ye-Lehmann S, Palmai Z, Amara N, Bigan E, Wydau S, et al. Redesigning the stereospecificity of tyrosyl-tRNA synthetase. *Proteins.* 2016;84:240–253.
14. Opuu V, Nigro G, Gaillard T, Mechulam Y, Schmitt E, Simonson T. Adaptive landscape flattening allows the design of both enzyme–substrate binding and catalytic power. *PLoS Comp Biol.* 2020;16:e1007600. doi:10.1371/journal.pcbi.1007600.
15. Villa F, Panel N, Chen X, Simonson T. Adaptive landscape flattening in amino acid sequence space for the computational design of protein–peptide binding. *J Chem Phys.* 2018;149:072302.
16. Mignon D, Druart K, Michael E, Opuu V, Polydorides S, Villa F, et al. Physics-based computational protein design: an update. *J Phys Chem A.* 2020;124:10637–10648.
17. Richter F, Leaver-Kay A, Khare SD, Bjelic S, Baker D. De novo enzyme design using Rosetta3. *PLoS One.* 2011;6:e19230.
18. Lechner H, Ferruz N, Hoecker B. Strategies for designing non-natural enzymes and binders. *Curr Opin Chem Biol.* 2018;47:67–76.
19. Stoddard B, editor. *Design and Creation of Ligand Binding Proteins.* vol. 1414 of *Methods Molec. Biol.* Springer Verlag, New York; 2016.
20. Michael E, Simonson T. How much can physics do for protein design? *Curr Opin Struct Biol.* 2022;72:46–54.
21. Wang FG, Landau DP. Efficient, multiple-range random walk algorithm to calculate the density of states. *Phys Rev Lett.* 2001;86:2050–2053.
22. Cornell W, Cieplak P, Bayly C, Gould I, Merz K, Ferguson D, et al. A second generation force field for the simulation of proteins, nucleic acids, and organic molecules. *J Am Chem Soc.* 1995;117:5179–5197.
23. Lopes A, Aleksandrov A, Bathelt C, Archontis G, Simonson T. Computational sidechain placement and protein mutagenesis with implicit solvent models. *Proteins.* 2007;67:853–867.

24. Michael E, Polydorides S, Simonson T, Archontis G. Simple models for nonpolar solvation: parametrization and testing. *J Comput Chem*. 2017;38:2509–2519.
25. Villa F, Mignon D, Polydorides S, Simonson T. Comparing pairwise-additive and many-body Generalized Born models for acid/base calculations and protein design. *J Comput Chem*. 2017;38:2396–2410.
26. Dahiyat BI, Mayo SL. De novo protein design: fully automated sequence selection. *Science*. 1997;278:82–87.
27. Gaillard T, Simonson T. Pairwise decomposition of an MMGBSA energy function for computational protein design. *J Comput Chem*. 2014;35:1371–1387.
28. Crépin T, Schmitt E, Mechulam Y, Sampson PB, Vaughan MD, Honek JF, et al. Use of analogues of methionine and methionyl adenylate to sample conformational changes during catalysis in *Escherichia coli* methionyl-tRNA synthetase. *J Mol Biol*. 2003;332:59–72.
29. Larson ET, Kim JE, Zucker FH, Kelley A, Mueller N, Napuli AJ, et al. Structure of *Leishmania major* methionyl-tRNA synthetase in complex with intermediate products methionyl adenylate and pyrophosphate. *Biochimie*. 2011;93:570–582.
30. Krivov GG, Shapalov MV, Dunbrack RL. Improved prediction of protein side-chain conformations with SCWRL4. *Proteins*. 2009;77:778–795.
31. Nigro G, Bourcier S, Lazennec-Schurdevin C, Schmitt E, Marlière P, , et al. Use of  $\beta$ -methionine as an amino acid substrate of *Escherichia coli* methionyl-tRNA synthetase. *J Struct Biol*. 2020;209:107435.
32. Jorgensen WL, Chandrasekar J, Madura J, Impey R, Klein M. Comparison of simple potential functions for simulating liquid water. *J Chem Phys*. 1983;79:926–935.
33. Phillips JC, Braun R, Wang W, Gumbart J, Tajkhorshid E, Villa E, et al. Scalable molecular dynamics with NAMD. *J Comput Chem*. 2005;26:1781–1802.
34. Tuffery P, Etchebest C, Hazout S, Lavery R. A new approach to the rapid determination of protein side chain conformations. *J Biomol Struct Dyn*. 1991;8:1267–1289.
35. Simonson T. The Proteus software for computational protein design. Ecole Polytechnique, Paris: <https://proteus.polytechnique.fr>; 2019.
36. Pokala N, Handel TM. Energy functions for protein design: adjustment with protein-protein complex affinities, models for the unfolded state, and negative design of solubility and specificity. *J Mol Biol*. 2005;347:203–227.



37. Schmitt E, Tanrikulu IC, Yoo TH, Panvert M, Tirrell DA, Mechulam Y. Switching from an Induced-Fit to a Lock-and-Key Mechanism in an Aminoacyl-tRNA Synthetase with Modified Specificity. *J Mol Biol.* 2009;394:843–851.
38. Mellot P, Mechulam Y, Le Corre D, Blanquet S, Fayat G. Identification of an amino acid region supporting specific methionyl-tRNA synthetase:tRNA recognition. *J Mol Biol.* 1989;208:429–443.
39. Schmitt E, Meinel T, Panvert M, Mechulam Y, Blanquet S. Two acidic residues of *Escherichia coli* methionyl-tRNA synthetase act as negative discriminants towards the binding of noncognate tRNA anticodons. *J Mol Biol.* 1993;233:615–628.
40. Guillon L, Schmitt E, Blanquet S, Mechulam Y. Initiator tRNA binding by e/aIF5B, the eukaryotic/archaeal homologue of bacterial Initiation Factor IF2. *Biochemistry.* 2005;44:15594–15601.
41. Braman J, Papworth C, A G. Site-directed mutagenesis using double-stranded plasmid DNA templates. *Methods Molec Biol.* 1996;57:31–44.
42. Schmitt E, Meinel T, Blanquet S, Mechulam Y. Methionyl-tRNA synthetase needs an intact and mobile KMSKS motif in catalysis of methionyl adenylate formation. *J Mol Biol.* 1994;242:566–577.
43. Mechulam Y, Dardel F, Lecorre D, Blanquet S, Fayat G. Lysine-335, part of the KMSKS signature sequence, plays a crucial role in the amino acid activation catalyzed by the methionyl-tRNA synthetase from *Escherichia coli*. *J Mol Biol.* 1991;217:465–475.
44. Hyafil F, Jacques Y, Fayat G, Fromant M, Dessen P, Blanquet S. Methionyl-tRNA synthetase from *Escherichia coli*: active stoichiometry and stopped flow analysis of methionyl adenylate formation. *Biochemistry.* 1976;15:3678–3685.
45. Mechulam Y, Schmitt E, Maveyraud L, Zelwer C, Nureki O, Yokoyama S, et al. Crystal structure of *Escherichia coli* methionyl-tRNA synthetase highlights species-specific features. *J Mol Biol.* 1999;294:1287–97.
46. Kabsch W. XDS. *Acta Cryst D.* 2010;66:125–132.
47. Collaborative Computational Project Number 4. The CCP4 suite: programs for protein crystallography. *Acta Cryst.* 1994;D50:760–776.
48. Adams PD, Afonine PV, Bunkoczi G, Chen VB, Davis IW, Echols N, et al. PHENIX: a comprehensive Python-based system for macromolecular structure solution. *Acta Cryst D.* 2010;66:213–221.

49. Emsley P, Lohkamp B, Scott WG, Cowtan K. Features and development of Coot. *Acta Cryst D*. 2010;66:486–501.
50. van den Bedem H, Wilson MA. Shining light on cysteine modification: connecting protein conformational dynamics to catalysis and regulation. *J Synchr Rad*. 2019;26:958–66.
51. Serre L, Verdon G, Choinowski T, Hervouet N, Risler JL, Zelwer C. How methionyl-tRNA synthetase creates its amino acid recognition pocket upon L-methionine binding. *J Mol Biol*. 2001;306:863–76.
52. Hayes RL, Vilseck JZ, Brooks III CL. Approaching protein design with multisite lambda dynamics: accurate and scalable mutational folding free energies in T4 lysozyme. *Prot Sci*. 2018;27:1910–1922.
53. Michael E, Polydorides S, Simonson T, Archontis G. Hybrid MC/MD for protein design. *J Chem Phys*. 2020;153:054113.